AIAA 80-1329R

Numerical Study of Flowfields About Asymmetric External Conical Corners

Manuel D. Salas*
NASA Langley Research Center, Hampton, Virginia

A numerical study of the flowfield about asymmetrical external axial corners formed by the juncture of swept compressive wedges is presented. The geometrical configuration allows a unified treatment of external corners typical of delta wings and rectangular inlets. The study investigates how the flow transitions from a symmetrical flowfield with a cross-flow stagnation point at the corner to an asymmetrical flowfield for which the flow spills over the corner. The effects of leading-edge sweep, wedge compression, and corner radius are investigated.

Introduction

THIS paper is the third and last report on a comprehensive study of flowfields about external conical corners. The corners considered are formed by the intersection of two compressive wedges. One of these wedges rests on the *xz* plane (see Fig. 1) and is defined in terms of a compression angle δ_1 and a leading-edge sweep angle Λ_1. The other wedge rests on a plane that is inclined Ω deg measured clockwise from the *yz* plane and is defined in terms of a compression angle δ_2 and a leading-edge sweep angle Λ_2. Through variations of these defining parameters, we can construct several configurations representative of geometric features found on high-speed aircraft, such as engine inlets, control surfaces, and delta wings. As simplifying assumptions, the wedges are considered to be infinite in extent and the freestream Mach number is assumed to be sufficiently high to support attached leading-edge shock waves. The resulting inviscid supersonic flowfield is thus conically self-similar with the conical origin at point 0 of Fig. 1. The region of interest is the region inside the Mach conoid emanating from the apex of the corner. This region is best studied by projecting the flowfield onto the surface of a unit sphere centered at the conical origin. The projection of the velocity vector onto this surface defines the cross-flow velocity vector and the cross-flow streamlines. The characteristic topological features of conical flows are revealed by these projections on the unit sphere. It is, however, more convenient to draw these vectors and curves on a plane surface; thus the results obtained on the unit sphere will be described after projection onto an *xy* plane. The boundaries defining the region are the two wedge surfaces, the bow shock wave, and the two cross-flow sonic lines, as shown in Fig. 2. Outboard of the cross-flow sonic lines, the flow is the known two-dimensional wedge flow corresponding to effective wedge angles $\bar{\delta}_{1,2} = \arctan(\tan\delta_{1,2}/\cos\Lambda_{1,2})$.

In the first paper[1] on this study, the structure of the flow was investigated from a theoretical point of view. In it the distinction was made between flowfields where the corner is a cross-flow stagnation point and flowfields where the flow spills over the corner. When the corner is a cross-flow stagnation point and the flow about the corner is symmetrical, a solution of the conical potential equation valid in a small neighborhood of the corner revealed that, for an external angle Φ (Fig. 1) less than 240 deg, the corner is a nodal point of streamlines. For external angles greater than 240 deg, the pressure distribution exhibits a weak singularity at the corner and the corner becomes a saddle point of streamlines with a nodal point of streamlines appearing on each wedge surface. This structure, with a node or saddle point of streamlines at the corner, which was labeled "symmetrical" in Ref. 1, may persist if the flow is only slightly asymmetrical.[2] For the spillover configuration, a set of equations valid at the corner was obtained which showed that the cross-flow experiences a rapid acceleration as it reaches the corner, attaining sonic conditions at the corner and then undergoing a conical analog

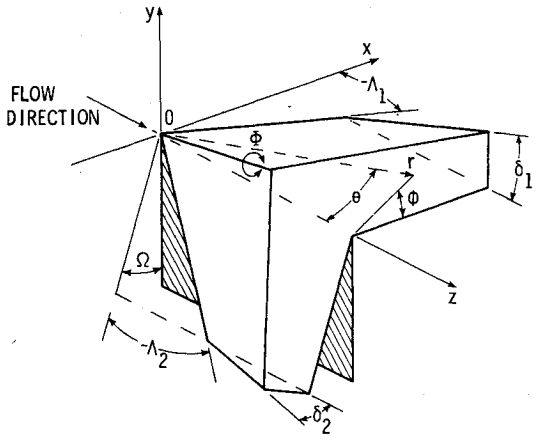

Fig. 1 Corner configuration.

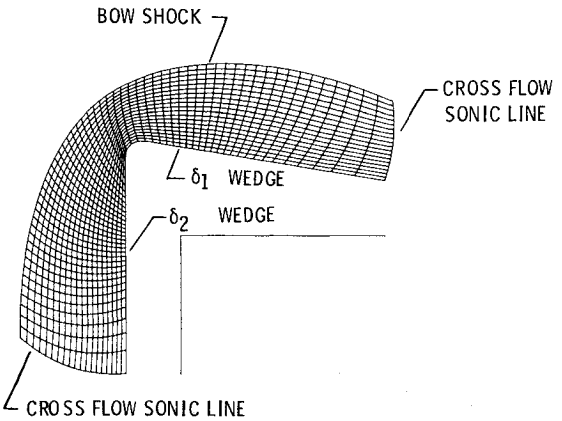

Fig. 2 Cross-flow plane with typical computational mesh.

Presented as Paper 80-1329 at the AIAA 13th Fluid and Plasma Dynamics Conference, Snowmass, Colo., July 14-16, 1980; submitted Sept. 16, 1980; revision received Jan. 15, 1982. This paper is declared a work of the U.S. Government and therefore is in the public domain.

*Research Scientist, Theoretical Aerodynamics Branch, Transonic Aerodynamics Division. Member AIAA.

of Prandtl-Meyer flow. This local analysis, however, gave no information on the size of the supersonic cross-flow bubble that forms at the corner. In the present study, we find that for the cases considered the cross flow becomes supersonic only in the immediate vicinity of the corner, with little effect away from the corner.

In the second paper[3] a numerical study of symmetrical configurations was conducted which confirmed the theoretical predictions of Ref. 1. In addition, a study of the effect of rounding the corner indicated that a nodal point of streamlines could be maintained at the corner, even for external angles greater than 240 deg, by increasing the corner radius r_0.

The pertinent literature has been reviewed in Refs. 1 and 3, and the interested reader is asked to consult these references.

In the present paper, asymmetrical configurations are investigated numerically. Of particular interest is the behavior of the flow as the configuration becomes more asymmetrical and the flow transitions from the stagnation corner to the spillover corner. Of the governing parameters γ, M_∞, Ω, $\Lambda_{1,2}$, $\delta_{1,2}$, and r_0, the first two, the adiabatic exponent and the freestream Mach number, have a quantitative rather than a qualitative effect on the flowfield, particularly as $M_\infty \to \infty$. For the present study, the values of γ and M_∞ will be 1.4 and 3, respectively. These are the same values used in Ref. 3. The effect of Ω on the flow is directly related to changes in the external angle Φ; and, as has already been mentioned, this determines the existence of a nodal or saddle point of streamlines when the cross flow stagnates at the corner. Since the effect of Ω was studied in detail in Ref. 3, we will limit our parametric studies here to the effects of the leading-edge sweep, the compression angle, and the radius of curvature of the corner.

Singular Points of Conical Streamlines

The equation describing the trajectories of cross-flow streamlines on the unit sphere is

$$\frac{d\theta}{d\phi} = \frac{v\sin\theta}{w} \tag{1}$$

where v and w are the velocity components in the θ and ϕ directions, respectively. A conical stagnation point (θ_0,ϕ_0) where v and w vanish is a singular point of Eq. (1). The theoretical formulation leading to the study of these singularities was initiated by Poincaré in his 1885 work on the equilibrium of a fluid in rotational motion.[4] Poincaré's analysis was applied to conical flows in Refs. 5-7. In this section, we will briefly review this work in order to develop the background necessary to understand the numerical results that will be presented later.

After taking into consideration the conical nature of the problem, the governing equations of motion on the unit sphere are

$$P_t + vP_\theta + \frac{wP_\phi}{\sin\theta} + \gamma\left(v_\theta + \frac{w_\phi}{\sin\theta} + 2u + v\cot\theta\right) = 0 \tag{2}$$

$$v_t + vv_\theta + \frac{wv_\phi}{\sin\theta} + \frac{a^2}{\gamma}P_\theta + uv - w^2\cot\theta = 0 \tag{3}$$

$$w_t + vw_\theta + \frac{ww_\phi}{\sin\theta} + \frac{a^2}{\gamma}\frac{P_\phi}{\sin\theta} + uw + vw\cot\theta = 0 \tag{4}$$

$$u_t + vu_\theta + \frac{wu_\phi}{\sin\theta} - v^2 - w^2 = 0 \tag{5}$$

$$S_t + vS_\theta + \frac{wS_\phi}{\sin\theta} = 0 \tag{6}$$

Here u is the velocity component in the radial direction, P is the natural logarithm of pressure, S is the entropy, and a is the speed of sound. The equations are written in their unsteady form for later reference; for the present analysis only the steady-state part is important. If we assume that the pressure is well behaved near a cross-flow stagnation point, we find that

$$v_\theta + w_\phi/\sin\theta + 2u = 0 \tag{7}$$

$$P_\theta = 0 \tag{8}$$

$$P_\phi = 0 \tag{9}$$

There are, however, pathological cases where the pressure is singular at the stagnation point (e.g., see Refs. 1 and 3), but these will not be considered.

Additional relations are obtained by differentiating the three momentum equations with respect to θ and ϕ. After some manipulation, we find

$$\left(\frac{v_\phi}{\sin\theta} - w_\theta\right)\left(v_\theta + \frac{w_\phi}{\sin\theta} + u\right) = 0 \tag{10}$$

$$\left(\frac{w_\theta v_\phi}{\sin\theta} - \frac{w_\phi v_\theta}{\sin\theta}\right)u_\phi = 0 \tag{11}$$

$$\left(\frac{w_\theta v_\phi}{\sin\theta} - \frac{w_\phi v_\theta}{\sin\theta}\right)u_\theta = 0 \tag{12}$$

The derivation of Eqs. (11) and (12) does not require that u be analytic at the stagnation point, but only that terms of order $vu_{\theta\theta}$, $wu_{\phi\phi}$, and the like vanish there. In view of Eq. (7) we can conclude, using Eq. (10), that

$$v_\phi/\sin\theta = w_\theta \tag{13}$$

Using Eqs. (7) and (13), the term in parentheses in Eqs. (11) and (12) may be written in the form $(w_\theta^2 + (v_\theta + u)^2 - u^2)$. Thus, at a cross-flow stagnation point, u_ϕ and u_θ must vanish, with a possible exception along the locus of points where

$$w_\theta^2 + (v_\theta + u)^2 - u^2 = 0 \tag{14}$$

We will come back to the significance of this relation shortly.

The nature of the singularity of Eq. (1) at a stagnation point (θ_0,ϕ_0) can be investigated by expanding the right-hand side of this equation in a Taylor series expansion about point (θ_0,ϕ_0). From this it follows[5,6] that the nature of the singularity depends on the roots $K_{1,2}$ of the characteristic equation

$$K^2 + hK + g = 0 \tag{15}$$

where

$$h = 2u \tag{16}$$

and

$$g = -(w_\theta^2 + (v_\theta + u)^2 - u^2) \tag{17}$$

It is easy to show that

$$h^2 - 4g = (v_\theta - w_\phi/\sin\theta)^2 + (v_\phi/\sin\theta + w_\theta)^2 \tag{18}$$

and since this term is the sum of square terms, the analysis predicts only nodal ($g>0$) and saddle ($g<0$) points of streamlines. Within the restrictions of the derivation of Eqs. (11) and (12), the vorticity vector ζ at a cross-flow stagnation point,

$$\zeta = (w_\theta - v_\phi/\sin\theta)\hat{r} + (u_\phi/\sin\theta)\hat{\theta} - u_\theta\hat{\phi} \tag{19}$$

must vanish, with a possible exception along the locus of points where Eq. (14) is satisfied. In addition to the nodal- and saddle-point singularities predicted by this analysis, other types of singularities of cross-flow streamlines, such as focal points, have been suggested in the literature (e.g., Ref. 8), but these involve unbounded w's that are not consistent with the total energy of the flow being bounded; hence these singularities are not considered in the analysis.

The nature of the singularity at a cross-flow stagnation point may also be examined by considering the isobar pattern at the stagnation point. When this analysis is performed,[16] we find that the characteristic equation for the isobars is

$$\bar{K}^2 + (P_{\theta\theta}P_{\phi\phi} - P_{\phi\theta}^2)/\sin^2\theta = 0 \tag{20}$$

The roots $\bar{K}_{1,2}$ of this equation depend on the sign of the determinant of the Hessian matrix,

$$\Delta = (P_{\theta\theta}P_{\phi\phi} - P_{\phi\theta}^2)/\sin^2\theta \tag{21}$$

introduced in Ref. 1.† From the previous discussion, it follows that, if the Hessian is positive, the isobars form a center point of pressure corresponding to a saddle point of streamlines; if the Hessian is negative, the isobars form a saddle point of pressure corresponding to a nodal point of streamlines. By differentiating the two cross-flow momentum equations with respect to θ and ϕ, the Hessian may be written in the form[1,6]

$$\Delta = (\gamma M^2)^2[\eta^2 + (\xi+1)^2][\eta^2 + (\xi+1)^2 - 1] \tag{22}$$

where M is the radial component of Mach number at the stagnation point and

$$\eta = w_\theta/u \tag{23}$$

$$\xi = v_\theta/u \tag{24}$$

are evaluated at the stagnation point. Equation (22) indicates that all nodal points must lie inside a circle of unit radius centered about the point $\eta = 0$, $\xi = -1$ in the η, ξ plane. All saddle points lie outside this circle. Points on the circle are known as critical or bifurcation points, because they signal major structural changes in the flow. The circle corresponds to the locus of points satisfying Eq. (14), where u_ϕ and u_θ might not vanish. The nature of the singularity on the circle is of a higher order than those investigated here.

Equation (22) may be further simplified by introducing the variables R, ω such that

$$\xi + 1 = \sqrt{R}\cos\omega \tag{25}$$

$$\eta = \sqrt{R}\sin\omega \tag{26}$$

The Hessian then is given by

$$\Delta = (\gamma M^2)^2 R(R-1) \tag{27}$$

If the singularity occurs on the surface of the wedge, then the vanishing of the normal velocity component on the wedge requires that

$$v - \frac{w}{\sin\theta}\frac{\partial\theta_w}{\partial\phi} = 0 \tag{28}$$

where $\theta_w = \theta_w(\phi)$ defines the intersection of the wedge with the unit sphere. If we differentiate this equation along the trace of the wedge surface on the unit sphere and evaluate the resulting expression at a cross-flow stagnation point, we find that

$$v_\phi + \left[v_\theta - \frac{\left(w_\phi + w_\theta \frac{\partial\theta_w}{\partial\phi} \right)}{\sin\theta} \right] \frac{\partial\theta_w}{\partial\phi} = 0 \tag{29}$$

Using Eqs. (7), (13), (23), and (24), we get

$$\tan\omega = \frac{\frac{-2}{\sin\theta}\frac{\partial\theta_w}{\partial\phi}}{1 - \left(\frac{1}{\sin\theta}\frac{\partial\theta_w}{\partial\phi}\right)^2} \tag{30}$$

which defines ω in terms of the wall geometry. The angle ω defines the orientation of the principal axes of the singularity.[6]

Numerical Formulation

The numerical solution to the present problem follows along the lines of the method used in Ref. 3. The time-dependent Euler equations, (2-6), are written in the computational space (X, Y, T) defined by

$$X = \frac{\phi_{sl}^2(Y) - \phi}{\phi_{sl}^2(Y) - \phi_{sl}^1(Y)} \tag{31}$$

$$Y = \frac{\theta - \theta_w(X)}{\theta_{sk}(X,T) - \theta_w(X)} \tag{32}$$

$$T = t \tag{33}$$

where $\theta_w(X)$ defines the location of the wall; $\phi_{sl}^{1,2}(Y)$ defines the location of the cross-flow sonic lines, with superscripts *1*, *2* referring to wedges δ_1, δ_2, respectively; and $\theta_{sk}(X,T)$ defines the location of the bow shock, which must be obtained as part of the solution. Limiting the computational domain to the region inboard of the cross-flow sonic lines has the advantage of concentrating mesh points in the region of interest (the flow outboard of the cross-flow sonic lines is known) and avoiding differentiation across the cross-flow sonic lines, where the flow variables are weakly singular. An even distribution of grid points in the computation plane XY results in the grid shown in Fig. 2.

The solution to the governing equations in the XYT space is obtained by integrating the equations in time using the MacCormack finite difference scheme until a steady state is reached.

As in Ref. 3, the radial momentum [Eq. (5)] was replaced by Bernoulli's equation and the integration of the entropy equation [Eq. (6)] was performed using windward differences[9] only. At a cross-flow stagnation point, the entropy equation degenerates to the form

$$S_T = 0 \tag{34}$$

This equation presented no particular problems at nodal points, but at saddle points, the value of the entropy on the body had to be extrapolated from the flowfield. The bow shock wave was computed as a discontinuity satisfying the Rankine-Hugoniot equations, using the procedure described in Ref. 3.

The inherent asymmetry in the MacCormack scheme was found to be a cause of errors. The asymmetry comes about because, in the predictor level of the scheme, the X derivatives of a point next to the cross-flow sonic line on wedge δ_2 are computed using the values on the sonic line; for the point next to the cross-flow sonic line on wedge δ_1, the values used are

†The $\sin^2\theta$ term was missing in the definition of Δ given in Ref. 1; therefore Eq. (9) of Ref. 1 should not have a factor of $\sin^2\theta$ on the right-hand side.

those on the second mesh point to the left of the sonic line. The opposite occurs in the corrector level. Since there are large gradients near the cross-flow sonic lines, the errors introduced by this asymmetry are quite large. The problem was overcome by switching the order of differentiation for the X derivatives at the midgrid point in the X direction in both the predictor and corrector levels. Perfectly symmetrical flowfield results were then obtained for symmetrical configurations, as shown in Fig. 3.

Results and Discussion

Results from several numerical calculations are presented to assess the effects of various geometrical asymmetries and of the radius of curvature of the corner. All calculations were made with 60 mesh points along the body and 20 mesh points between body and shock. For most cases, 500 time steps were required to reach a steady state, needing approximately 300 CPU seconds on a CDC Cyber-175 computer.

The symmetrical configuration shown in Fig. 3, corresponding to $\delta_1 = \delta_2 = 10$ deg, $\Lambda_1 = \Lambda_2 = 0$ deg, and $r_0 = 0.05$, is taken as the baseline configuration. Symmetrical departures from this configuration were presented in Ref. 3. For most cases discussed, plots of the cross-flow streamlines and isobar contours, similar to those in Fig. 3, will be presented.

The cross-flow streamline trajectories were obtained by integrating Eq. (1), from the shock to the body, in the computational plane using the equivalent of a second-order Runge-Kutta method. The results were then mapped back to the physical plane. The cross-flow streamlines wet the body surface only at saddle and nodal points, and these are labeled with an S and an N, respectively. The typical vortical layer associated with these conical flows is clearly visible on the plots.

Leading-Edge Effect

Sweeping the leading edge back has a minor effect on the flowfield structure. Figure 4 shows the computed flowfield after sweeping the leading edge of the δ_1 wedge back 30 deg ($\Lambda_1 = -30$ deg). As shown in the figure, the locations of the stagnation points are not very different from those of the symmetrical case, Fig. 3. Sweeping the leading edges forward has a more significant effect. For the symmetrical configuration, if the leading edges are swept forward, a cross-flow shock forms outboard of the cross-flow sonic line. For the asymmetrical configuration with only one leading edge swept forward, the cross-flow shock is not required, since the three-dimensional streamlines do not have to turn parallel to a symmetry plane. As shown in Fig. 5, with the leading edge of the δ_1 wedge swept forward 20 deg, the saddle point moves toward the nodal point on the δ_1 wedge, which results in more flow spilling over the corner toward the other node. If the leading-edge sweep is increased to 30 deg, as in Fig. 6, the saddle point and the nodal point on the δ_1 wedge disappear, leaving behind only the nodal point on the δ_2 wedge. All the cross flow from the δ_1 wedge now spills over the corner. A plot of R as a function of Λ_1 (Fig. 7) shows that the bifurcation value of Λ_1 (that value at which the flow structure changes from three singular points to one) occurs at about 23 deg for this configuration. At this critical value of Λ_1, the saddle and node points come together, forming a higher-order singularity. For swept-back leading edges the values of R for the two nodes are so close that they appear as a single line in Fig. 7.

The effect of the leading edge can be understood by noting that both types of sweeps produce the same pressure levels at

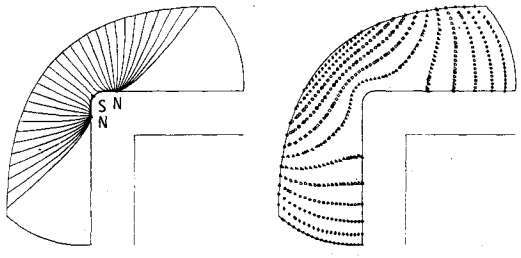

Fig. 3 Symmetrical baseline configuration; $\delta_{1,2} = 10$ deg, $\Lambda_{1,2} = 0$ deg, $r_0 = 0.05$, $M_\infty = 3$. Cross-flow streamlines on the left and corresponding isobar pattern on the right.

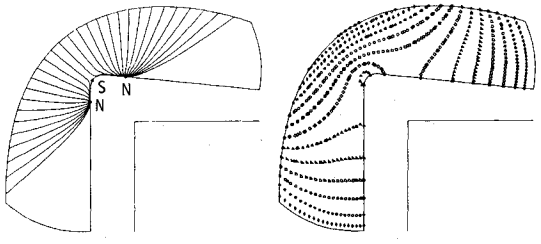

Fig. 4 Effect of leading-edge sweep-back; $\delta_{1,2} = 10$ deg, $\Lambda_1 = -30$ deg, $\Lambda_2 = 0$ deg, $r_0 = 0.05$, $M_\infty = 3$.

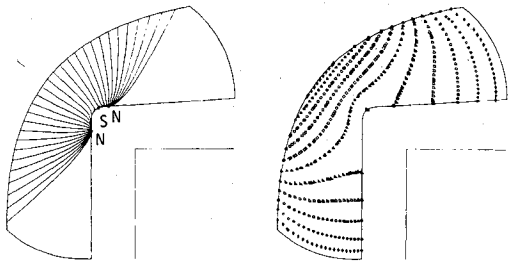

Fig. 5 Effect of leading-edge sweep-forward; $\delta_{1,2} = 10$ deg, $\Lambda_1 = 20$ deg, $\Lambda_2 = 0$ deg, $r_0 = 0.05$, $M_\infty = 3$.

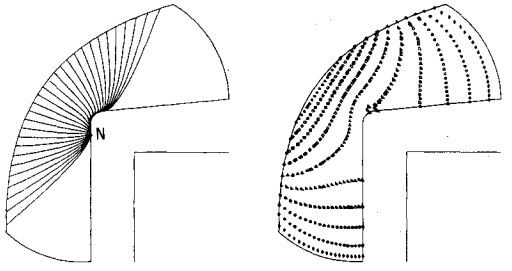

Fig. 6 Effect of leading-edge sweep-forward; $\delta_{1,2} = 10$ deg, $\Lambda_1 = 30$ deg, $\Lambda_2 = 0$ deg, $r_0 = 0.05$, $M_\infty = 3$.

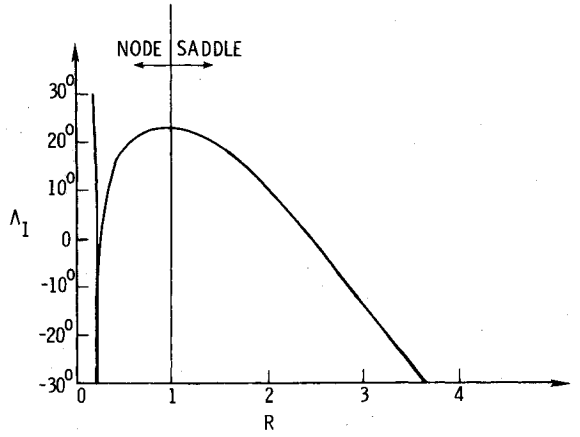

Fig. 7 Behavior of the singular points with leading-edge sweep. Bifurcation occurs at about $\Lambda_1 = 23$ deg.

the cross-flow sonic line, since the effect is related to the $\cos(\Lambda_{1,2})$. Turning the leading edge back turns the three-dimensional streamline away from the corner, whereas forward sweep turns the three-dimensional streamline toward the corner, increasing the likelihood of cross-flow spillover.

Compression-Angle Effect

To investigate the compression-angle effect, we will start from the case shown in Fig. 4: this is the base configuration with the δ_1 leading edge swept back 30 deg. A decrease of 1 deg in the δ_1 angle produces the results shown in Fig. 8. The flow is spilling from wedge δ_2 to wedge δ_1, and the node on wedge δ_2 and the saddle point are practically on top of each other. If the compression angle is decreased by one more degree (Fig. 9), the saddle and nodal points on wedge δ_2 disappear and all the cross flow now converges on the nodal point on wedge δ_1. An increase in the compression angle δ_1 (to 16 deg) has, as expected, the opposite effect, as shown in Fig. 10. The saddle point now moves toward the node on wedge δ_2, as shown in the figure. A plot of the cross-flow velocity on the surface (assumed positive from left to right) in Fig. 11 clearly shows what is happening as δ_1 is changing. The basic shape of cross-flow distribution allows for three roots when $q=0$; as δ_1 is changed, the curve is displaced up or down, making two of the roots imaginary for values of δ_1 outside the two bifurcation values. The behavior on the $\delta_1 R$ plane is shown in Fig. 12 by the curve with corner radius equal to 0.05. The bifurcation values occur at $\delta_1^* \sim 9$ deg and $\delta_1^{**} \sim 14.2$ deg. The difference $\delta_1^{**} - \delta_1^*$ is a measure of the compression needed to have the flow spill from one wedge surface to the other. For values of δ_1 greater than 16 deg and smaller than 8 deg, the value of R approaches $R=0$. The fact that there are no solutions for $R<0$ is a result of the nonexistence of focal points.

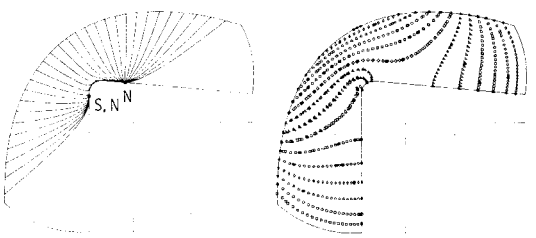

Fig. 8 Effect of compression angle; $\delta_1 = 9$ deg, $\Lambda_1 = -30$ deg, $\delta_2 = 10$ deg, $\Lambda_2 = 0$ deg, $r_0 = 0.05$, $M_\infty = 3$.

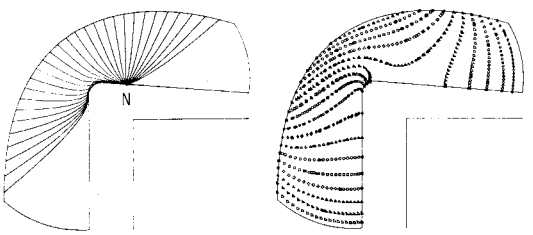

Fig. 9 Effect of compression angle; $\delta_1 = 8$ deg, $\Lambda_1 = -30$ deg, $\delta_2 = 10$ deg, $\Lambda_2 = 0$ deg, $r_0 = 0.05$, $M_\infty = 3$.

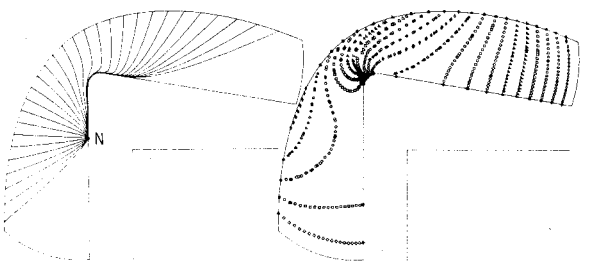

Fig. 10 Effect of compression angle; $\delta_1 = 16$ deg, $\Lambda_1 = -30$ deg, $\delta_2 = 10$ deg, $\Lambda_2 = 0$ deg, $r_0 = 0.05$, $M_\infty = 3$.

Corner-Radius Effect

In Ref. 3 it was shown that, as the corner radius was increased on a symmetrical configuration, the node-saddle-node structure was replaced with the single-node structure. For asymmetrical configurations, it is evident from Fig. 12 that, as the corner radius increases, the amount of compression $\delta_1^{**} - \delta_1^*$ needed for the flow to spill from one wedge to the other decreases. The bifurcation value r_0^* occurs at about 0.11; for values of r_0 greater than this value, only a single nodal point is observed. The flowfield shown in Fig. 13 for the configuration $\delta_1 = 10.5$ deg and $r_0 = 0.1$ is near critical values of both δ_1 and r_0. With a slight perturbation of these parameters, the flowfield changes character, as shown in Fig. 14 for $r_0 = 0.12$. The effect of increasing the corner radius on the cross-flow velocity on the body surface can be seen by comparing Figs. 15 and 16. It is speculated that, for a configuration with simultaneous bifurcation values of r_0 and δ_1, the cross-flow velocity on the surface will vanish within a region of the rounded corner. The resulting flowfield will then

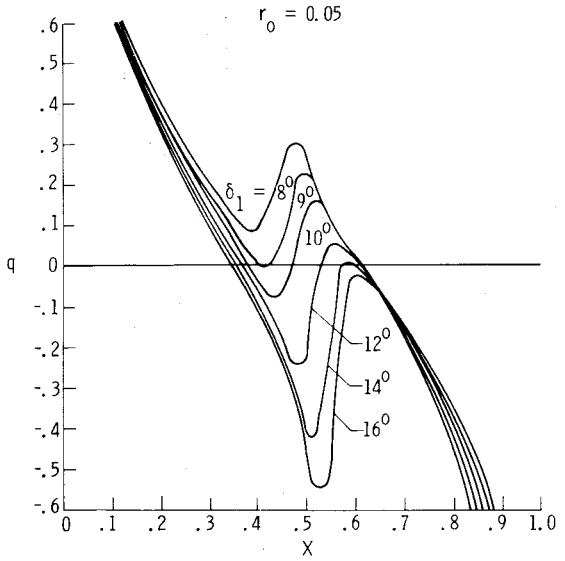

Fig. 11 Effect of compression angle on surface cross-flow velocity. The possibility for three real roots at $q=0$ is evident from the figure.

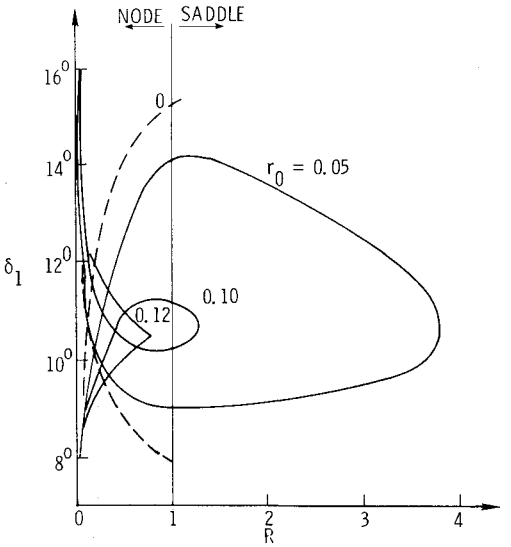

Fig. 12 Behavior of the singular points with compression angle and corner radius.

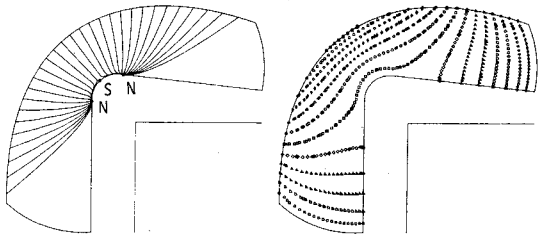

Fig. 13 Flowfield structure near bifurcation values of δ_1 and r_0; $\delta_1 = 10.5$ deg, $\Lambda_1 = -30$ deg, $\delta_2 = 10$ deg, $\Lambda_2 = 0$ deg, $r_0 = 0.10$, $M_\infty = 3$.

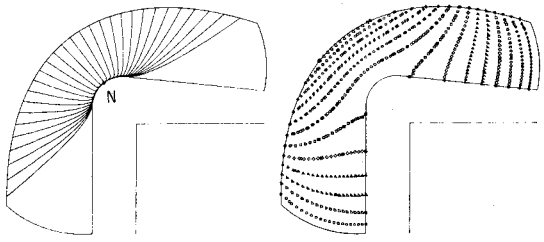

Fig. 14 Flowfield structure near bifurcation values of δ_1 and r_0; $\delta_1 = 10.5$ deg, $\Lambda_1 = -30$ deg, $\delta_2 = 10$ deg, $\Lambda_2 = 0$ deg, $r_0 = 0.12$, $M_\infty = 3$.

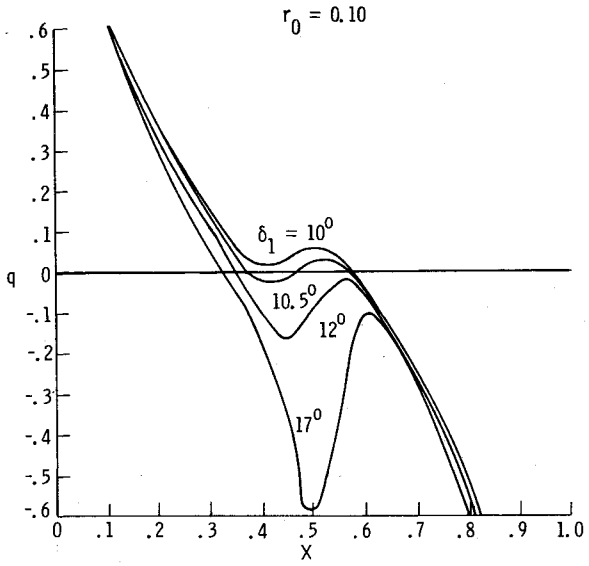

Fig. 15 Effect of compression angle and corner radius on surface cross-flow velocity; $r_0 = 0.10$.

be similar to the degenerate case of a circular cone at zero incidence (see Fig. 5 of Ref. 5).

Sharp Corner

For sharp corners, with a stagnation point on the corner, the pressure behaves like[1]

$$p \sim \chi^{4\pi/\Phi - 2} \tag{35}$$

where χ is the angular distance from the corner. For external angles Φ greater than 240 deg, $\partial p/\partial \chi$ is infinite at the corner and the stagnation point is a saddle point. The value of R in this case goes to $+\infty$. If the configuration is made asymmetrical, the saddle point moves from the corner toward the nodal point with the highest pressure level; at the corner the flow then spills toward the other nodal point. The amount of compression $\delta_1^{**} - \delta_1^*$ for the saddle point to move from one nodal point to the other increases as $r_0 \to 0$ (dashed line in Fig. 12), so the effect of a sharp corner is to retard the appearance of the single-node structure. It seems that, to within the accuracy of the calculations, the saddle point tolerates a small amount of asymmetry in the flow before moving from the corner; this is in agreement with the observations of Ref. 2. The values of R for the saddle-point singularity off the corner, for the cases tested, were an order of magnitude greater than the scale used in Fig. 12; thus they do not show in the figure.

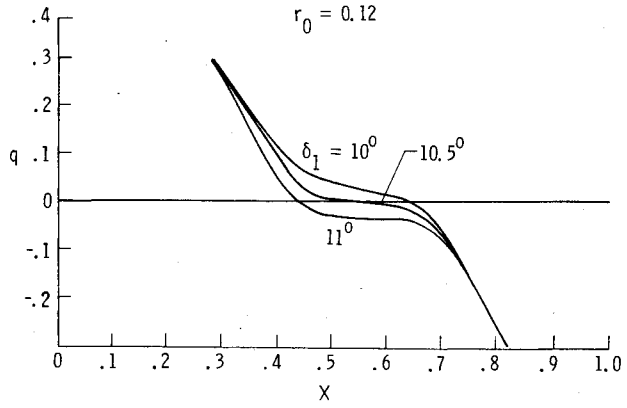

Fig. 16 Effect of compression angle and corner radius on surface cross-flow velocity; $r_0 = 0.12$. Note how flat q becomes at $\delta_1 = 10.5$ deg.

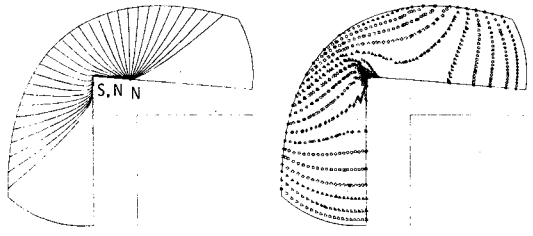

Fig. 17 Effect of sharp corner on flow structure; $\delta_1 = 8$ deg, $\Lambda_1 = -30$ deg, $\delta_2 = 10$ deg, $\Lambda_2 = 0$ deg, $r_0 = 0$, $M_\infty = 3$.

It was shown in Ref. 1 that, once the flow spills over the sharp corner, the cross flow becomes sonic at the corner and then undergoes a conical Prandtl-Meyer expansion, with the possibility of a recompression cross-flow shock occurring at the corner. In the early phases of the present study, the corner point was treated as a special point where the conical Prandtl-Meyer expansion fan was enforced as a boundary condition. For all cases tested with this provision, we found that the supersonic cross flow was immediately recompressed, confining the supersonic cross flow to the corner point. Since the gradients that develop at the corner when the Prandtl-Meyer fan is enforced are severe and a very fine grid is needed to prevent wiggles from forming, this boundary condition was removed. The resulting flowfield for a sharp-corner case with streamline pattern near the transition from the triple-stagnation-point structure to the single-stagnation-point structure is shown in Fig. 17.

Conclusions

The effects of various parameters on the flowfield of external, axial, conical corners have been investigated. The effect of sweeping the leading edges forward is to produce spilling over the corner from the high-pressure wedge to the low-pressure wedge. Sweeping the leading edges back has only a minor effect on the flow. Increasing the compression angle of one wedge relative to the other increases the spillage from the high-pressure side to the low-pressure side. Finally, the effect of increasing the corner radius of curvature is to facilitate the transition from the triple-stagnation-point structure to the single-stagnation-point structure.

References

[1]Salas, M. D. and Daywitt, J., "Structure of the Conical Flowfield About External Axial Corners," *AIAA Journal*, Vol. 17, Jan. 1979, pp. 41-47.

[2]Kutler, P., Pulliam, T. H., and Vigneron, Y. C., "Computation of the Viscous Supersonic Flow over Symmetrical and Asymmetrical External Axial Corners," AIAA Paper 78-1135, July 1978.

[3]Salas, M. D., "Careful Numerical Study of Flowfields About Symmetrical External Conical Corners," *AIAA Journal*, Vol. 18, June 1980, pp. 646-651.

[4]Poincaré, H., "Sur l'équilibre d'une masse fluide animée d'un mouvement de rotation," *Acta Mathematica*, Vol. 7, Sept. 1885, pp. 259-380.

[5]Smith, J.H.B., "Remarks on the Structure of Conical Flows," *Progress in Aerospace Sciences*, Vol. 12, Pergamon Press, New York, 1972, pp. 241-272.

[6]Bakker, P. G., "Conical Streamlines and Pressure Distribution in the Vicinity of Conical Stagnation Points in Isentropic Flow," Delft Univ. of Technology, the Netherlands, Rept. LR-244, April 1977.

[7]Bakker, P. G., Bannink, W. J., and Reyn, J. W., "Potential Flow Near Conical Stagnation Points," *Journal of Fluid Mechanics*, Vol. 105, 1981, pp. 239-260.

[8]Guiraud, J. P. and Zeytounian, R. Kh., "A Double-Scale Investigation of the Asymptotic Structure of Rolled-Up Vortex Sheets," *Journal of Fluid Mechanics*, Vol. 79, Pt. 1, 1977, pp. 93-112.

[9]Moretti, G. and Pandolfi, M., "Analysis of the Inviscid Flow About a Yawed Cone—Preliminary Studies," Polytechnic Institute of Brooklyn, New York, PIBAL Rept. 72-18, May 1972.